
Nonlinear dynamics of a bladed dual-shaft

Marion Gruin^{*,} — Fabrice Thouverez^{*} — Laurent Blanc^{*}
Pierrick Jean^{**}**

** Laboratoire de Tribologie et Dynamique des Systèmes - UMR CNRS 5513
École Centrale de Lyon
36 avenue Guy de Collongue, F-69134 Ecully cedex
{marion.gruin, fabrice.thouverez, laurent.blanc}@ec-lyon.fr*

*** Snecma - SAFRAN Group, Site de Villaroche
Rond Point René Ravaud-Réau
F-77550 Moissy-Cramayel
pierrick.jean@snecma.fr*

ABSTRACT. In the industrial context of performance improvement of dual-shaft aircraft engines, experimental results demonstrate how important it is to consider the influence of the dynamics of the high pressure (HP) shaft on the response of the bladed disk located on the low pressure (LP) shaft. Indeed, this coupling seems to play an important role in the design purposes in rotating machinery industry as it can have a significant impact on the dynamic behaviour of turbomachines. The model developed here consists of a HP shaft and a LP bladed shaft connected by an intershaft bearing. Nonlinear features of this intershaft bearing require the development of specific nonlinear algorithms. Thus, this paper aims at coupling the two modelling levels in order to grasp the nonlinear vibratory phenomena of a bladed dual-shaft under unbalances.

RÉSUMÉ. Dans le contexte actuel d'amélioration des performances des turboréacteurs, des résultats d'essais montrent qu'il est nécessaire de considérer, dès la conception, l'influence de la dynamique de l'arbre haute pression (HP) sur les aubages de l'arbre basse pression (BP). Le modèle développé est un modèle bi-rotor composé d'un arbre HP et d'un arbre BP, connectés entre eux par un palier interarbre, avec sur l'arbre BP, un modèle simplifié de roue aubagée. Les caractéristiques hautement non linéaires du palier interarbre vont nécessiter la mise en place d'algorithmes de résolution non linéaires adaptés. Ainsi, le travail s'appuie sur la simulation combinée d'un problème de dynamique d'ensemble avec celui plus spécifique des roues aubagées afin d'évaluer la réponse dynamique non linéaire du système couplé.

KEYWORDS: nonlinear dynamics, rotor, bearing, contact.

MOTS-CLÉS : dynamique non linéaire, rotor, roulement, contact.

DOI:10.3166/EJCM.20.207-225 © 2011 Lavoisier, Paris

1. Introduction

Because most rotating machines operate more and more at their design limits, there is an increase of the dynamic couplings between the different parts of the engine. For matters of high machine efficiency, optimized multi-shafts are used in rotating machinery. This leads to systems where several unbalances are simultaneously present. Moreover, in the context of dual-shaft aircraft engine, the interaction between both the dynamics of shafts and that of bladed disks calls into question the commonly used design criteria. Usually, rotordynamics relies on simplified models of propulsion organs (Lalanne *et al.*, 1998), while bladed disks are studied with full Finite Element models in rotating machinery industry. This work offers to couple these two modelling levels.

Furthermore, one source of nonlinearities in multi-rotors systems concerns the use of rolling intershaft bearing that involves radial clearance and nonlinear contact stiffness (Harris *et al.*, 1973). Indeed, it is well known that the nonlinear bearing may drastically influence the dynamic behaviour of rotating systems (Choi *et al.*, 1987; Tiwari *et al.*, 2000). One of the most widely used approaches to obtain the nonlinear response of such a system is the numerical integration procedure, like shooting methods (Sundararajan *et al.*, 1997). Nevertheless, this approach requires large resources in terms of computational time for systems involving a large number of degrees of freedom or strong nonlinearities. Thus, the most popular alternative methods used to estimate the nonlinear response of the system are the frequency methods, which provide a nonlinear solution approximated by truncated Fourier series. The Harmonic Balance Method and continuation schemes (Narayanan *et al.*, 1998; Cameron *et al.*, 1989; Nacivet *et al.*, 2003) have become over the last few decades the favourite tool to study strongly nonlinear dynamics.

In this paper, our interest will be in the development of our own model coupling a dual-shaft system with a simplified bladed disk model. We also propose to study the unbalance responses of this system with a radial clearance and stiffness contact located in the intershaft bearing. For that purpose, the paper is divided into four parts. The definition of the simplified model of the bladed dual-shaft is firstly described in the rotating frame by using an energy formulation. Secondly, the basic concept of the Harmonic Balance Method is introduced with the path following continuation scheme and the nonlinearities involved in the model are described. The third part presents several numerical results. A linear analysis is investigated to validate the bladed dual-shaft model and nonlinear studies are carried out to assess the influence of nonlinearities on the response of the system. Eventually, the last part draws some conclusions and suggests possible new developments.

2. Bladed dual-shaft system

2.1. Description of the system

The HP and the LP rotors are both composed of a shaft modelled by an Euler-Bernoulli beam connected to several rigid disks modelled by concentrated masses with rotational inertia. These shafts are set on compliant bearings at multiple locations and connected by an intershaft bearing (Guskov *et al.*, 2007). The bladed disk considered in the model is located on the LP rotor, see Figure 1, where (x, y, z) denotes the rotating frame. This model is inspired from an existing model (Sinha, 2004). A full set of flexible blades also modelled by Euler-Bernoulli beams is clamped on the LP rigid disk, see Figure 3.

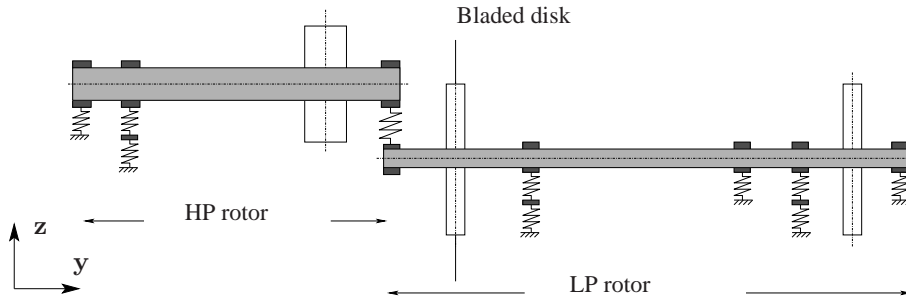


Figure 1. Bladed dual-shaft model

2.2. Dual-shaft model

The developed analytical model of the dual-shaft relies on an energy formulation. For the analytical formulation, the energies and the potentials of the shafts have to be defined. The kinetic energy is expressed in the global frame as follows:

$$T_i = \frac{1}{2} \int_{\Omega} \rho \dot{\mathbf{x}}_i^T \dot{\mathbf{x}}_i d\Omega \quad [1]$$

where i denotes either the high pressure (HP) rotor or the low pressure (LP) rotor and \mathbf{x} represents the displacement vector expressed in the global frame. In the full model, a bladed disk is introduced on the LP shaft. The displacements of the LP rotor are described in its own rotating frame in order to avoid time-dependent terms resulting from the periodicity of rotating structure. Thus, the LP shaft kinetic energy is defined by:

$$T_{LP} = \frac{1}{2} \int_{\Omega} \rho \dot{\mathbf{u}}_{lp}^T \dot{\mathbf{u}}_{lp} d\Omega + \int_{\Omega} \rho \dot{\mathbf{u}}_{lp}^T \boldsymbol{\Omega}_{lp} \mathbf{u}_{lp} d\Omega + \frac{1}{2} \int_{\Omega} \rho \mathbf{u}_{lp}^T \boldsymbol{\Omega}_{lp}^T \boldsymbol{\Omega}_{lp} \mathbf{u}_{lp} d\Omega \quad [2]$$

where \mathbf{u}_{lp} is the displacement vector of the LP rotor in its rotating frame and $\mathbf{\Omega}_{lp}$ is the transition matrix from the global frame to the LP rotating frame. We assumed that there are no bladed disks on the HP rotor in order to simplify the model description. Consequently, the HP rotor equations can be projected in the LP rotating frame and the kinetic energy has the following expression:

$$\begin{aligned} T_{HP/LP} = & \frac{1}{2} \int_{\Omega} \rho \dot{\mathbf{u}}_{hp}^T \dot{\mathbf{u}}_{hp} d\Omega + \int_{\Omega} \rho \dot{\mathbf{u}}_{hp}^T \mathbf{\Omega}_{hp}^{lp} \mathbf{u}_{hp} d\Omega + \int_{\Omega} \rho \dot{\mathbf{u}}_{hp}^T \mathbf{\Omega}_{hp} \mathbf{u}_{hp} d\Omega \\ & + \int_{\Omega} \rho \mathbf{u}_{hp}^T \mathbf{\Omega}_{hp}^{lpT} \mathbf{\Omega}_{hp} \mathbf{u}_{hp} d\Omega + \frac{1}{2} \int_{\Omega} \rho \mathbf{u}_{hp}^T \mathbf{\Omega}_{hp}^{lpT} \mathbf{\Omega}_{hp}^{lp} \mathbf{u}_{hp} d\Omega \\ & + \frac{1}{2} \int_{\Omega} \rho \mathbf{u}_{hp}^T \mathbf{\Omega}_{hp}^T \mathbf{\Omega}_{hp} \mathbf{u}_{hp} d\Omega \end{aligned} \quad [3]$$

where \mathbf{u}_{hp} is the HP displacement vector, $\mathbf{\Omega}_{hp}$ the transition matrix from the global frame to the HP rotating frame and $\mathbf{\Omega}_{hp}^{lp}$ the transition matrix from the HP rotating frame to the LP rotating frame. The rigid disks are characterized by their inertia data which are also expressed in the LP rotating frame.

Besides, the elastic strain of each rotor is defined by a potential energy associated with its bending:

$$V_{int_i} = \frac{1}{2} \int_0^{l_i} E_i I_i \mathbf{u}_i''^T \mathbf{u}_i'' dy \quad [4]$$

with E_i , I_i and l_i being the Young's modulus, the second moment of area and the length of each rotor, respectively.

The bearings and the intershaft bearing are introduced through a potential associated with their stiffness and a function of dissipation associated with their damping. More precisely, the potential expression associated with the intershaft bearing stiffness is defined by:

$$V_{bearing} = \frac{1}{2} \Delta \mathbf{u}(y_{inter})^T \mathbf{K}_{inter} \Delta \mathbf{u}(y_{inter}) \quad [5]$$

where $\Delta \mathbf{u}(y_{inter}) = \mathbf{u}_{hp}(y_{inter}) - \mathbf{u}_{lp}(y_{inter})$.

Two directions of displacement are considered for each shaft as two orthogonal translations in the disks plane. The transverse displacements u_i and w_i are defined using a Rayleigh-Ritz approximation:

$$\mathbf{u}_i(y, t) = \begin{cases} u_i(y, t) = \sum_{m=0}^{m_{tot}} U_m^i(t) V_m^i(y) \\ w_i(y, t) = \sum_{m=0}^{m_{tot}} W_m^i(t) V_m^i(y) \end{cases} \quad [6]$$

where y denotes the abscissa along the shaft, m_{tot} is the number of Ritz functions considered to describe the shaft bending. $V_m^i(y)$ represents the displacement polynomial shape function associated with each rotor.

2.3. Bladed disk simplified model

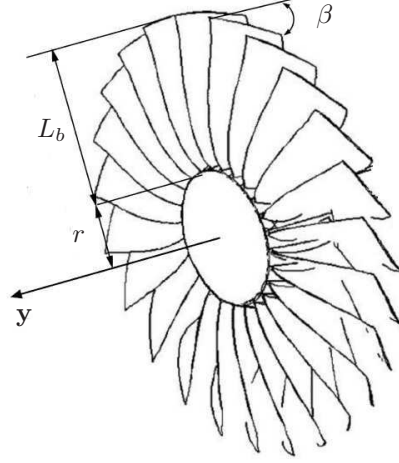


Figure 2. Bladed disk

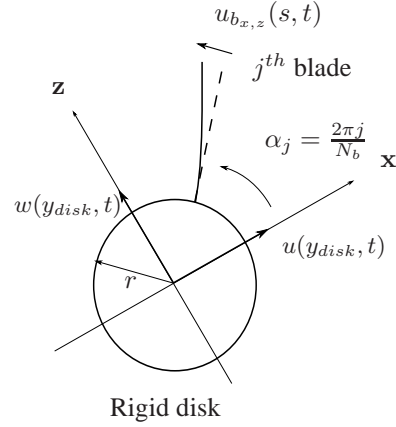


Figure 3. Bladed disk model

Since an energy formulation is used to develop this model in the LP rotating frame, the kinetic energy T_b^j of the j^{th} blade can be defined as follows:

$$T_b^j = \int_0^{L_b} \frac{1}{2} \rho_b S_b \mathbf{v}_{S/R_0}^T(G) \mathbf{v}_{S/R_0}(G) ds + \int_0^{L_b} \frac{1}{2} \boldsymbol{\omega}_{S/R_0}^T \mathbf{I} \boldsymbol{\omega}_{S/R_0} ds \quad [7]$$

where $\mathbf{v}_{S/R_0}(G)$ and $\boldsymbol{\omega}_{S/R_0}$ are the speed and the rotation of the mass center of a blade cross section, respectively. \mathbf{I} is the blade inertia matrix defined in its inertial frame. R_0 denotes the global frame, s the abscissa along the blade, ρ_b and S_b are the density and the area of a blade cross section, respectively.

As for shafts, a potential energy associated with the elastic strain of blades is defined by:

$$V_{int_b} = \frac{1}{2} \int_0^{L_b} E_b I_b \left(u_b''(s, t) \right)^2 ds \quad [8]$$

where E_b is the Young's modulus of elasticity of the blade, I_b is the blade second moment of area for flexure and u_b the displacement vector of a blade.

Moreover, a pre-stress potential has been defined in order to take the centrifugal effects into account in the model:

$$V_{cen_b} = \frac{1}{2} \int_0^{L_b} \rho_b S_b \Omega_{lp}^2 \left(\frac{(r + L_b)^2 - (s + r)^2}{2} \right) u_b'^2(s, t) ds \quad [9]$$

with Ω_{lp} the rotation speed of the LP rotor and r the bladed disk radius.

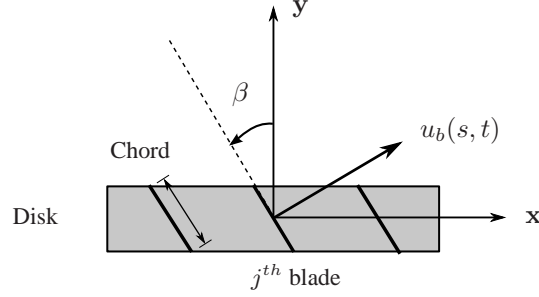


Figure 4. Top view of the bladed rigid disk

Only one direction of displacement for each blade is considered to represent its deflection $u_b^j(s, t)$. It is assumed that the minor principal moment of inertia of the blade cross section coincides with the chord direction. Thus, the blade lateral deflection $u_b(s, t)$ under pure bending moment takes place in the direction normal to the chord. The interested reader can refer to (Sinha, 2004) for details. This deflection is defined using a Rayleigh-Ritz approximation as follows:

$$u_b^j(s, t) = \sum_{n=1}^{n_{tot}} X_n^j(t) Y_n^j(s) \quad [10]$$

where n_{tot} denotes the number of functions considered for the bending of the j^{th} blade. $Y_n^j(s)$ represents the displacement shape function which satisfy the clamping condition at the blade attachment and its expression is:

$$Y_n(s) = \sin(a_n s) + b_n s + c_n s^2 \quad [11]$$

$$\text{with } \begin{cases} a_n = \frac{(2n-1)\pi}{2L_b}, \\ b_n = -a_n, \\ c_n = \left(\frac{b_n^2}{2}\right) \sin(b_n L_b). \end{cases} \quad [12]$$

Then, the Lagrange equations of the full dynamic system of the bladed dual-shaft take the following matrix form:

$$\mathbf{M} \ddot{\mathbf{q}} + (\mathbf{D} + \mathbf{G}) \dot{\mathbf{q}} + (\mathbf{K} + \mathbf{N} + \mathbf{P}) \mathbf{q} = \mathbf{0} \quad [13]$$

In this expression, \mathbf{M} , \mathbf{D} , \mathbf{G} , \mathbf{K} , \mathbf{N} and \mathbf{P} are the mass matrix, the damping matrix, the gyroscopic matrix, the stiffness matrix, the spin softening matrix, and the circulatory matrix, respectively.

The generalized vector $\mathbf{q}(t)$ is the combination of all degrees of freedom and can be written as:

$$\mathbf{q}(t) = \left[U_0^{hp}(t) W_0^{hp}(t) \cdots U_{m_{tot}}^{hp}(t) W_{m_{tot}}^{hp}(t) U_0^{lp}(t) W_0^{lp}(t) \cdots U_{m_{tot}}^{lp}(t) W_{m_{tot}}^{lp}(t) X_1^1(t) \cdots X_{n_{tot}}^1(t) \cdots X_1^{N_b}(t) \cdots X_{n_{tot}}^{N_b}(t) \right]^T \quad [14]$$

where N_b represents the total number of blades.

3. Nonlinear dynamics

3.1. Equation governing the system and definition of nonlinearities

The full model (cf. Section 2) consists in two shafts connected by a linear intershaft bearing with a bladed disk rigidly linked to the LP shaft; this model is linear at this stage. In order to grasp the complex dynamics of such a system, nonlinearities coming from bearings have to be considered. In this study, the nonlinearity is introduced on the intershaft bearing which connects the LP and the HP shaft dynamics. The equation governing the dynamic behaviour of the system with the unbalance excitations and the nonlinear forces can be formulated as:

$$\mathbf{M} \ddot{\mathbf{q}} + \tilde{\mathbf{C}} \dot{\mathbf{q}} + \tilde{\mathbf{K}} \mathbf{q} + \mathbf{F}_{nl}(\mathbf{q}) = \mathbf{F}_u \quad [15]$$

where $\tilde{\mathbf{C}} = \mathbf{D} + \mathbf{G}$ and $\tilde{\mathbf{K}} = \mathbf{K} + \mathbf{N} + \mathbf{P}$ are the generalized damping and stiffness matrices, respectively. $\mathbf{F}_{nl}(\mathbf{q})$ represents the nonlinear force vector and \mathbf{F}_u the external force vector (HP or LP unbalance).

The model used to define the nonlinearity located on the intershaft bearing consists in a clearance and a contact nonlinear stiffness involving four generalized degrees of freedom.

Let us consider the relative displacement vector of the intershaft bearing:

$$\Delta \mathbf{u} = \begin{pmatrix} u_{hp} - u_{lp} \\ w_{hp} - w_{lp} \end{pmatrix} \quad [16]$$

where the displacement values are taken at the intershaft bearing abscissa. Then, the nonlinear force vector defining the contact force is described by:

$$\mathbf{F}_{nl}(\Delta \mathbf{u}) = k_{nl} (\|\Delta \mathbf{u}\| - \delta) \mathcal{H}(\|\Delta \mathbf{u}\| - \delta) \frac{\Delta \mathbf{u}}{\|\Delta \mathbf{u}\|} \quad [17]$$

where k_{nl} and δ are the nonlinear stiffness and the radial clearance value, respectively. $\mathcal{H}(\cdot)$ represents the Heaviside's function and $\|\Delta \mathbf{u}\| = \sqrt{\Delta u^2 + \Delta w^2}$. This nonlinear force defines a bilateral clearance in the intershaft bearing. Its projection on the x axis is illustrated in Figure 5. In order to obtain the periodic solution of the nonlinear bladed dual-shaft system, the Harmonic Balance Method is one of the most widespread methods thanks to its affordable computational cost.

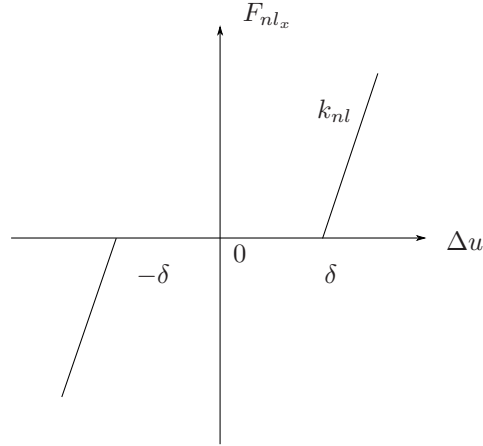


Figure 5. Representation of the nonlinear force

3.2. Numerical methods for the nonlinear resolution

3.2.1. The harmonic balance method

The main idea of this method consists in assuming that the solution $\mathbf{q}(t)$ of the motion equation [15] is searched as a periodic function with the same period T as the excitation. Indeed, the solution can be approximated by truncated Fourier series of order N , with $\omega = \frac{2\pi}{T}$ the fundamental frequency:

$$\mathbf{q}(t) \approx \mathbf{a}_0 + \sum_{k=1}^N (\mathbf{a}_k \cos(k\omega t) + \mathbf{b}_k \sin(k\omega t)) \quad [18]$$

where \mathbf{a}_0 , \mathbf{a}_k and \mathbf{b}_k define the Fourier coefficients which are the new unknowns of the system. As the solution is assumed to be a periodic function with the same period as the unbalance forces, the nonlinear force vector can also be approximated by Fourier series truncated in the same order N , that reads:

$$\mathbf{F}_{nl} \approx \mathbf{c}_0 + \sum_{k=1}^N (\mathbf{c}_k \cos(k\omega t) + \mathbf{d}_k \sin(k\omega t)) \quad [19]$$

The calculation of the harmonic nonlinear coefficients \mathbf{c}_0 , \mathbf{c}_k , \mathbf{d}_k will be described in section 3.2.3. Once the approximations [18] and [19] have been substituted in the motion equation [15], a Galerkin projection of this motion equation over the trigonometric basis $(1, \cos(\omega t), \sin(\omega t), \dots, \cos(N\omega t), \sin(N\omega t))$ leads to a system of $(2N + 1)n_{dof}$ nonlinear algebraic equations (where n_{dof} is the number of degrees of freedom for the bladed dual-shaft system):

$$\mathbf{A}\mathbf{x}_h + \mathbf{F}_{nl_h}(\mathbf{x}_h) = \mathbf{F}_{u_h} \quad [20]$$

where \mathbf{F}_{u_h} and \mathbf{F}_{nl_h} are the projections of the excitation and the nonlinear terms over the trigonometric basis, respectively. \mathbf{A} represents the dynamic stiffness corresponding to each harmonic component:

$$\mathbf{A} = \begin{bmatrix} \mathbf{A}^0 & 0 & \cdots & 0 \\ 0 & \mathbf{A}^1 & \cdots & 0 \\ \vdots & \vdots & \ddots & \vdots \\ 0 & 0 & \cdots & \mathbf{A}^N \end{bmatrix} \quad [21]$$

$$\text{with } \begin{cases} \mathbf{A}^0 = \tilde{\mathbf{K}}; \\ \mathbf{A}^k = \begin{bmatrix} \tilde{\mathbf{K}} - (k\omega)^2 \mathbf{M} & (k\omega) \tilde{\mathbf{C}} \\ -(k\omega) \tilde{\mathbf{C}} & \tilde{\mathbf{K}} - (k\omega)^2 \mathbf{M} \end{bmatrix}, \text{ for } k = 1, \dots, N. \end{cases} \quad [22]$$

Eventually, the nonlinear algebraic system [20] can be solved by a Newton-like method.

3.2.2. The path following continuation

The Harmonic Balance Method is coupled with a path following continuation technique. This approach allows to follow the evolution of the system with respect to a chosen control parameter denoted by μ . In that case, this parameter is the rotation speed Ω_{lp} of the LP rotor as the dynamic response is sought in a rotation speed range of the LP rotor which is known.

A predictor-corrector algorithm is used to determine the solution pair (\mathbf{x}_h, μ) . Here we assume that one solution point (\mathbf{x}_h^i, μ^i) of the response curve is already known, where \mathbf{x}_h^i is the solution vector of the Fourier coefficients and μ^i denotes the chosen control parameter. The predictor algorithm considered in this study is the tangent predictor which provides an estimation of the following solution point calculated from the previous solution (\mathbf{x}_h^i, μ^i) . Then, this estimation is used as a starting point for the correction algorithm. A Newton-Raphson algorithm is employed to determine the solution pair $(\mathbf{x}_h^{i+1}, \mu^{i+1})$. By using the arc-length continuation procedure (Nayfeh *et al.*, 1995; Kim *et al.*, 2005), the estimated solution has to verify the hypersphere equation of radius Δs :

$$\Delta s^{i+1} = \sqrt{\|\mathbf{x}_h^{i+1} - \mathbf{x}_h^i\|^2 + (\mu^{i+1} - \mu^i)^2} \quad [23]$$

Finally, the Newton-like correction algorithm employed to solve the augmented system of nonlinear equations [20] and [23] leads to the solution pair $(\mathbf{x}_h^{i+1}, \mu^{i+1})$. The step size Δs is adjusted according to the convergence of previous steps.

3.2.3. Determination of the harmonic nonlinear coefficients

The nonlinearity defined in Section 3.1 is strong and non-smooth. In order to establish the implicit relation $\mathbf{F}_{nl}(\Delta \mathbf{u})$ between the nonlinear force and the relative

displacement vector and its projection $\mathbf{F}_{nl_h}(\mathbf{x}_h)$ into the frequency space, an Alternating Frequency/Time domain strategy (AFT) is employed (Cameron *et al.*, 1989). This one can be represented by the following scheme:

$$\mathbf{x}_h = \begin{pmatrix} \mathbf{a}_0 \\ \mathbf{a}_1 \\ \mathbf{b}_1 \\ \vdots \\ \mathbf{a}_N \\ \mathbf{b}_N \end{pmatrix} \xrightarrow{FFT^{-1}} \mathbf{q}(t) \rightarrow \mathbf{F}_{nl}(\mathbf{q}) \xrightarrow{FFT} \mathbf{F}_{nl_h} = \begin{pmatrix} \mathbf{c}_0 \\ \mathbf{c}_1 \\ \mathbf{d}_1 \\ \vdots \\ \mathbf{c}_N \\ \mathbf{d}_N \end{pmatrix} \quad [24]$$

The starting point of this method is an estimation of Fourier coefficients vector \mathbf{x}_h . Then, an inverse Fast Fourier Transform (FFT) procedure is employed to determine the approximated temporal displacement $\mathbf{q}(t)$ which is used to evaluate the nonlinear forces in the time domain. Finally, an FFT procedure is applied on these forces in order to obtain the harmonic coefficients \mathbf{c}_0 , \mathbf{c}_k and \mathbf{d}_k of the nonlinear contribution.

4. Numerical simulations

As explained previously, the bladed dual-shaft system studied here is composed of two rotors supported by a set of bearings and an intershaft bearing. These shafts are connected to several rigid disks and to a simplified bladed disk model located on the LP shaft. All the parametric values for the complete model are given in Table 1. In this section, linear and nonlinear studies of the bladed dual-shaft will be presented. First, a linear analysis is carried out. This analysis details the balanced rotors behaviour to extract the modal elements. Unbalanced linear behaviour is then exposed for future comparison with unbalanced nonlinear behaviour. In a second time, the nonlinear intershaft bearing model is used. Unbalanced responses are then built and compared to the linear ones.

4.1. Linear analysis of the model

4.1.1. Modal analysis

The linear analysis of the bladed dual-shaft system without any unbalances allows to get mode shapes and classical Campbell diagram. The mode shapes are studied at null speed and represented in Figure 6. The intershaft bearing is located in the abscissa $y = 0$, the position of the HP rotor is displayed in the negative abscissas, whereas that of the LP rotor is spotted in the positive abscissas. The frequency of the first mode is $f_1 = 27$ Hz, it is mainly a dual-shaft mode with a low participation of blades. The second mode at $f_2 = 41$ Hz is mainly a LP rotor mode especially at the rigid disk location. The blades dynamics is negligible on this mode shape. The third mode is identified as a pure blades mode and all the blades vibrate at the same frequency

Table 1. Parametric values of the bladed dual-shaft system

Notation	Description	Value
l_{hp}	Length of the HP shaft	1 m
d_{hp}	Diameter of the HP shaft	0,05 m
$y_{disk_{hp}}$	Abscissa of the HP disk	-0,2 m
$y_{bearing_{hp}}^1$	Abscissa of the HP bearing 1	-1 m
$y_{bearing_{hp}}^2$	Abscissa of the HP bearing 2	-0,9 m
$K_{bearing_{hp}}^1$	HP flexible coupling stiffness	$4,3 \cdot 10^4$ N/m
$K_{bearing_{hp}}^2$	HP rolling bearing stiffness	$3 \cdot 10^6$ N/m
l_{lp}	Length of the LP shaft	1,7 m
d_{lp}	Diameter of the LP shaft	0,04 m
$y_{disk_{lp}}^1$	Abscissa of the LP disk 1	0,1 m
$y_{disk_{lp}}^2$	Abscissa of the LP disk 2	1,5 m
$y_{bearing_{lp}}^1$	Abscissa of the LP bearing 1	0,2 m
$y_{bearing_{lp}}^2$	Abscissa of the LP bearing 2	1,2 m
$y_{bearing_{lp}}^3$	Abscissa of the LP bearing 3	1,4 m
$y_{bearing_{lp}}^4$	Abscissa of the LP bearing 4	1,7 m
$K_{bearing_{lp}}^1$	LP rolling bearing stiffness 1	$1,5 \cdot 10^7$ N/m
$K_{bearing_{lp}}^2$	LP rolling bearing stiffness 2	$1 \cdot 10^9$ N/m
$K_{bearing_{lp}}^3$	LP rolling bearing stiffness 3	$1 \cdot 10^7$ N/m
$K_{bearing_{lp}}^4$	LP flexible coupling stiffness	$4,3 \cdot 10^4$ N/m
$E_{hp,lp}$	Young's modulus of rotors	$210 \cdot 10^9$ N/m ²
$\rho_{hp,lp}$	Density of rotors	7800 kg/m ³
$m_{tot_{hp,lp}}$	Number of Ritz functions for rotors	6
y_{inter}	Abscissa of the intershaft bearing	0 m
K_{inter}	Intershaft bearing stiffness	$1 \cdot 10^9$ N/m
N_b	Total number of blades	4
L_b	Length of blades	0,17 m
E_b	Young's modulus of blades	$114 \cdot 10^9$ N/m ²
ρ_b	Density of blades	4500 kg/m ³
β	Incidence angle of blades	60°
n_{tot}	Number of Ritz functions for blades	2

$f_3 = 51$ Hz. Finally, the last studied mode at $f_4 = 78$ Hz is a strongly coupled mode between the dual-shaft and the blades.

The evolution of the eigen frequencies of the system as a function of the rotation speed of the LP rotor give us a Campbell diagram, see Figure 7. This one is represented in the rotating frame in LP precession. The bladed dual-shaft is fully axisymmetric implying that the eigen frequencies are double at null speed. On the one hand, the eigen frequencies f_1 , f_2 and f_4 open with respect to the rotation speed which is characteristic of gyroscopic effects of rotors. On the other hand, the frequencies of blades modes (f_3) increase with respect to the rotation speed. This feature is due to the centrifugal effects which have been introduced in the model, see equation [9]. Besides, equations being written in the rotating frame the negative slope curves are forward

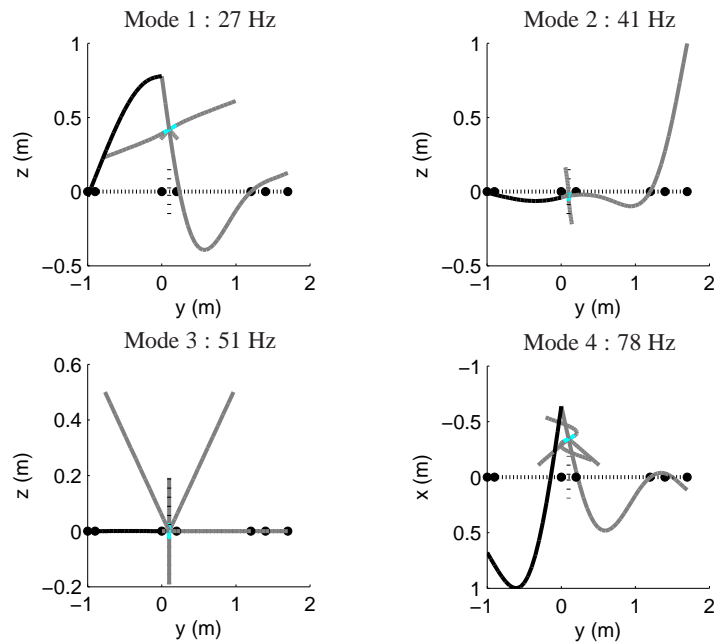


Figure 6. Mode shapes of the system - (—) HP rotor, (---) LP rotor with blades and (•) bearings location

modes, whereas the positive slope curves are backward modes. The frequency of the synchronous excitation of the LP rotor can be read on the abscissa axis $f = 0$ because the system is observed in the LP rotating frame. The intersections of forward modes with the abscissa axis define the critical speeds for LP unbalance. The dashed line represents the frequency of the synchronous excitation of the HP rotor $f = \Omega_{hp} - \Omega_{lp}$ in the LP rotating frame. In the same way, the intersections of this line with forward modes define critical speeds for HP unbalance. The critical speeds of the forward modes are summarized in Table 2. The ratio of the rotation speed of the HP rotor to that of the LP rotor is $\frac{\Omega_{hp}}{\Omega_{lp}} = 2.8$.

4.1.2. Linear unbalance responses

As the rotordynamical system model is axisymmetric, only the forward modes are supposed to respond to the unbalance excitation (Lalanne *et al.*, 1998). In the speed range $\Omega_{lp} = [0; 2200]$ rpm, the linear forced response curves with respect to unbalance forces are shown in Figure 8 for the relative displacement of the intershaft bearing. On the one hand, the LP unbalance excitation is a constant force in the LP rotating frame. The dashed curve represents the LP unbalance response of the intershaft bearing. One

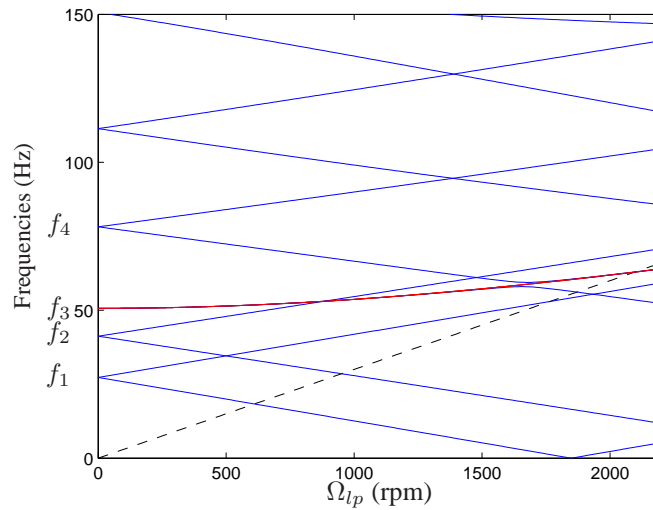


Figure 7. Campbell diagram - Evolution of (—) dual-shaft and (—) blades natural frequencies according to the LP rotation speed, (- - -) Synchronous excitation of the HP rotor in the LP frame

Table 2. Critical speeds of the bladed dual-shaft

Modes	Critical speeds (rpm)	
	LP unbalance	HP unbalance
1	1850	610
2	—	960
3	—	2110
4	—	1870

can observe that only the first mode is excited by the LP unbalance in the studied speed range. On the other hand, the HP unbalance excitation is a harmonic force in the LP frame. Furthermore, it is important to notice that the first four modes are all excited in this speed range. The blade tip displacement is also illustrated in Figure 9 with respect to the HP and the LP unbalances.

4.2. Nonlinear studies

Here, the nonlinear unbalance responses due to the nonlinear intershaft bearing will be investigated. Various cases of excitation will be considered, namely the LP unbalance, the HP unbalance and both unbalances.

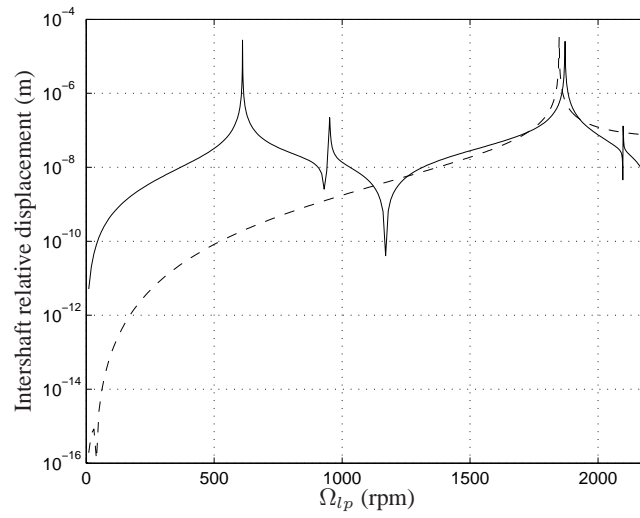


Figure 8. Linear responses of the intershaft bearing - (—) HP and (- - -) LP unbalance excitation

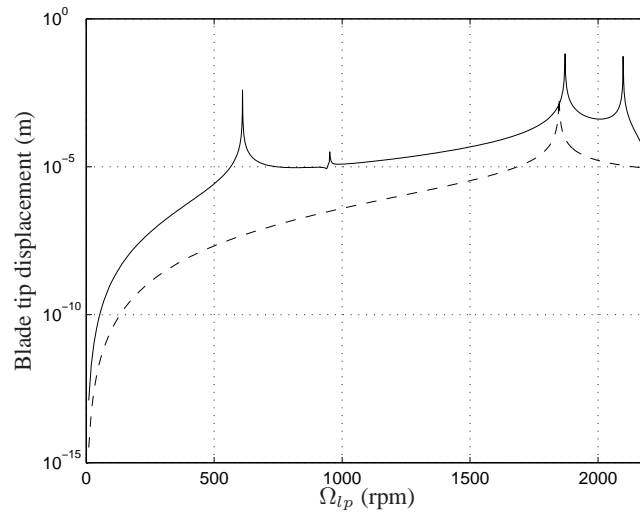


Figure 9. Linear responses of the blade tip - (—) HP and (- - -) LP unbalance excitation

4.2.1. LP unbalance response of the nonlinear system

Now, let us consider the nonlinear dynamics of the bladed dual-shaft subjected to a LP unbalance. The unbalance is located on the bladed disk at the distance $d = r_{disk}$ and the unbalance mass value is $m_u = 50 \text{ g}$. Only the first mode is observed in this case because only this one is excited in the studied rotation speed range. The radial clearance value introduced in the model is $\delta = 10 \mu\text{m}$ corresponding to a worn bearing. Figure 10 shows a zoom of the nonlinear LP unbalance response curve around the first peak which is located at $\Omega_{lp} = 1850 \text{ rpm}$. The number of the harmonic components retained in the solution for all the nonlinear results is equal to one because the harmonic components become less significant for upper orders. First, the evolution of the relative intershaft displacement with respect to the rotation speed Ω_{lp} is described on Figure 10(a) and highlights the nonlinear behaviour of the bladed dual-shaft. Indeed, for displacement values which are inferior to the clearance value, the nonlinear and linear response curves merge. When the clearance value is reached, one can observe that the contribution of the nonlinear terms of the intershaft bearing changes the behaviour of the system. In the same way, the blade tip response shown in Figure 10(b) has been studied. This analysis also highlights the sensitivity of its behaviour to the nonlinear intershaft bearing. This phenomenon observed on the peak indicates the “hardening effect” of the nonlinearity. This effect implies an increase of the frequency and, consequently, an increase of the critical speed.

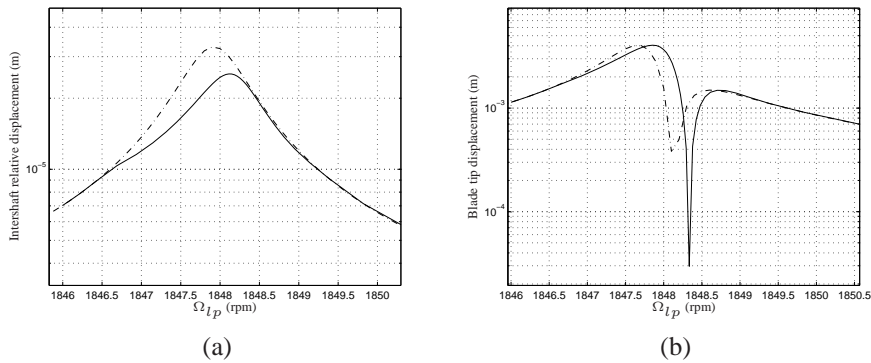


Figure 10. (- · -) Linear and (—) nonlinear LP unbalance responses of mode 1 with the nonlinear intershaft bearing - (a) Relative displacement of the intershaft bearing and (b) Blade tip displacement

4.2.2. HP unbalance response of the nonlinear system

The nonlinear dynamics of the system subjected to an HP unbalance excitation has also been analysed. The unbalance is located on the HP disk at $d = r_{disk}$ and the unbalance mass value is also $m_u = 50 \text{ g}$. In order to compare the HP unbalance response to the previous study, the first mode is observed and the clearance introduced in the model has the same value $\delta = 10 \mu\text{m}$. Figure 11 displays a zoom of the nonlinear

HP unbalance response curve around the first peak which is located at $\Omega_{lp} = 610$ rpm. The same kind of observations can be drawn with respect to the previous case. The relative intershaft displacement curve shown in Figure 11(a) indicates that the behaviour is modified when the clearance is consumed. Moreover, an analysis of the blade tip response, see Figure 11(b), has been carried out and tends to show the influence of the “hardening effect” of the nonlinearity on the peak. Consequently, the frequency and the critical speed values increase.

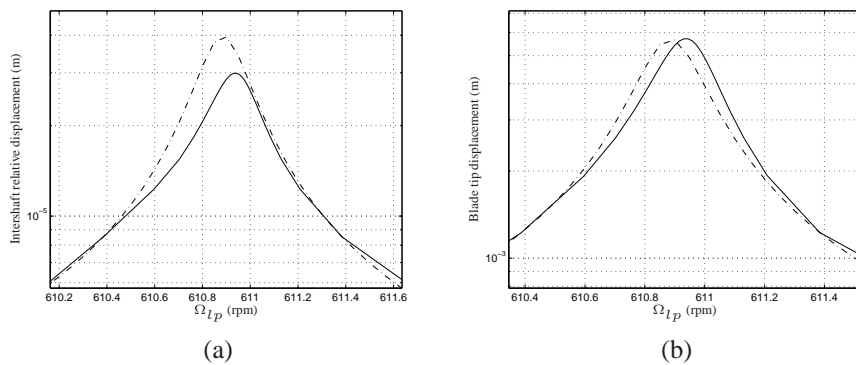


Figure 11. (---) Linear and (—) nonlinear HP unbalance responses of mode 1 with the nonlinear intershaft bearing - (a) Relative displacement of the intershaft bearing and (b) Blade tip displacement

It is important to note that the HP unbalance response of mode 2 has not been analysed in the present work because the intershaft bearing displacement is negligible on this mode shape, see Figure 6. Similarly, the coupled mode (mode 4) has been investigated with the same parameters for the unbalance mass and the clearance value. A zoom of the nonlinear response of both the intershaft relative displacement and the blade tip displacement around the rotation speed $\Omega_{lp} = 1870$ rpm is represented in Figure 12(a) and Figure 12(b), respectively. One can observe the nonlinear behaviour when the amplitude reaches the clearance value $\delta = 10 \mu m$. Indeed, the peak of the nonlinear response curve is located at a higher frequency than that of the linear response curve. Thus, the response of the bladed dual-shaft system has been performed on the one hand for the LP unbalance and on the other hand for the HP unbalance in the rotation speed range $\Omega_{lp} = [0; 2200]$ rpm. These last remarks emphasise the interaction between the dynamics of both the dual-shaft and the blades.

4.2.3. Response of the nonlinear system with both unbalances

In this section, the LP and HP unbalance responses of the system are analysed considering both excitations at the same time. The analytical formulation has been fully developed in the LP rotating frame (cf. Section 2). In this specific frame, the

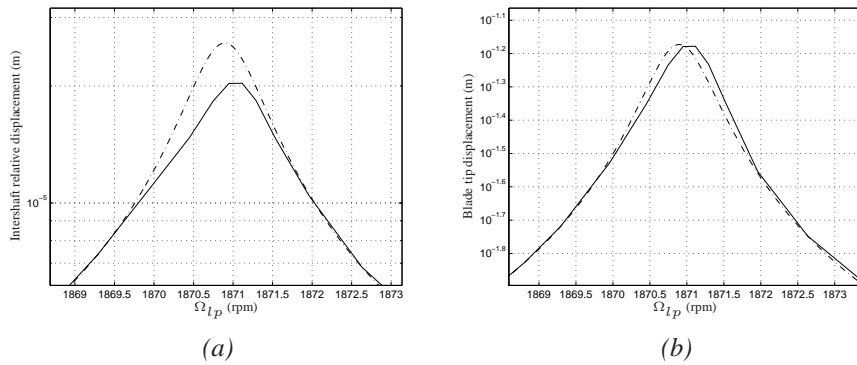


Figure 12. (- - -) Linear and (—) nonlinear HP unbalance responses of mode 4 with the nonlinear intershaft bearing - (a) Relative displacement of the intershaft bearing and (b) Blade tip displacement

LP unbalance excitation can be seen as a constant force whereas the HP unbalance is considered as a harmonic force with $\omega = \Omega_{hp} - \Omega_{lp}$ the fundamental frequency. During the Galerkin projection procedure, these unbalance forces are projected over the trigonometric basis (cf. Section 3). Therefore, the LP unbalance excitation is the constant part of the vector \mathbf{F}_{u_h} and the HP unbalance excitation is developed on the harmonic components of the same vector \mathbf{F}_{u_h} .

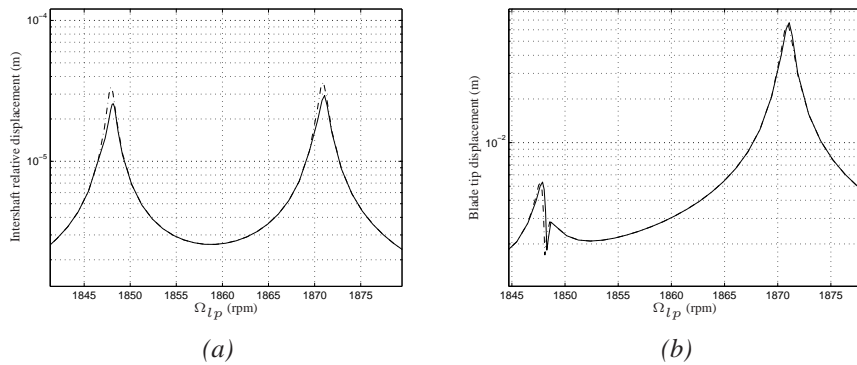


Figure 13. (- - -) Linear and (—) nonlinear unbalances responses with the nonlinear intershaft bearing - (a) Relative displacement of the intershaft bearing and (b) Blade tip displacement

On the linear forced response shown in Figure 8, the contribution of both excitations is observed in the speed range $\Omega_{lp} = [1800; 1900]$ rpm. Then, Figure 13 shows a zoom of the nonlinear response of the bladed dual-shaft system. The same parameters have been chosen for the unbalance masses $m_{u_{lp}} = m_{u_{hp}} = 50$ g and the clearance

value $\delta = 10 \mu m$. The global response has the same behaviour as the LP unbalance response (see Figure 10) for the first peak and the same behaviour as the HP unbalance response of the mode 4 (see Figure 12) for the second peak. Therefore, one can conclude that the basic Harmonic Balance Method is well-suited to study the nonlinear response of the system under both unbalance excitations.

5. Conclusions

A full bladed dual-shaft model has been developed in the rotating frame. The gyroscopic effects, the spin softening effects and the centrifugal effects have been taken into account, leading to a complete system from a phenomenological and physical point of view. This model allows to assess the interaction between blades dynamics and dual-shaft dynamics through mode couplings which have been observed.

Besides, the study of the dynamic behaviour of this complex system involving nonlinearities has been carried out. The nonlinearity has been introduced in the intershaft bearing which is a crucial organ connecting the dynamics of both rotors. The nonlinear force model includes a contact nonlinear stiffness and a clearance. The Harmonic Balance Method coupled with an arc-length continuation technique has been implemented in order to analyse the bladed dual-shaft system with a nonlinear intershaft bearing. As the considered nonlinearity is strong and non-smooth, an AFT procedure has been developed to obtain the nonlinear forced response. On the response curves, the influence of the nonlinearity has been identified through a hardening effect on the response around the peak. The introduction of a nonlinear intershaft bearing has allowed to investigate the excitability of the blades located on the LP rotor subjected to HP unbalance excitations.

It would be interesting to investigate more harmonic components in the Fourier decomposition in order to study the influence of the approximation on the global response of such a system. Avenues for future research work would consist in taking more realistic blades models into account. At first, an extension of this work would be to replace the simplified bladed disk model by a full Finite Element model more representative of the blades geometry. Eventually, the multi-stage cyclic symmetry techniques (Laxalde *et al.*, 2007) may also be examined in order to consider several bladed disks on the dual-shaft model.

Acknowledgements

Thanks go to Snecma for its technical and financial support. This work takes place in the framework of the MAIA mechanical research and technology program sponsored by CNRS, ONERA and SAFRAN Group.

6. References

- Cameron T., Griffin J., “ An Alternating Frequency/Time Domain Method for Calculating the Steady-State Response of Nonlinear Dynamic Systems”, *Journal of Applied Mechanics*, vol. 56, n° 1, p. 149-154, 1989.
- Choi Y., Noah S., “ Nonlinear steady state response of a rotor-support system”, *ASME Journal of Vibration, Acoustics, Stress and Reliability in Design*, vol. 109, p. 255-261, 1987.
- Guskov M., Sinou J.-J., Thouverez F., Naraikin O. S., “ Experimental and Numerical Investigations of a Dual-Shaft Test Rig with Intershaft Bearing”, *International Journal of Rotating Machinery*, 2007.
- Harris T., Mindel M., “ Rolling element bearing dynamics”, *Wear*, vol. 23, n° 3, p. 311-337, 1973.
- Kim T., Rook T., Singh R., “ Super- and sub-harmonic response calculations for a torsional system with clearance nonlinearity using the harmonic balance method”, *Journal of Sound and Vibration*, vol. 281, n° 3-5, p. 965-993, 2005.
- Lalanne M., Ferraris G., *Rotordynamics Prediction in Engineering*, Wiley, 1998.
- Laxalde D., Thouverez F., Lombard J.-P., “ Dynamical analysis of multi-stage cyclic structures”, *Mechanics Research Communications*, vol. 34, n° 4, p. 379-384, 2007.
- Nacivet S., Pierre C., Thouverez F., Jezequel L., “ A dynamic Lagrangian frequency-time method for the vibration of dry-friction-damped systems”, *Journal of Sound and Vibration*, vol. 265, n° 1, p. 201-219, 2003.
- Narayanan S., Sekar P., “ A frequency domain based numeric-analytical method for non-linear dynamical systems”, *Journal of Sound and Vibration*, vol. 211, n° 3, p. 409-424, 1998.
- Nayfeh A. H., Balachandran B., *Applied non-linear dynamics. Analytical, computational and experimental methods*, John Wiley & Sons, 1995.
- Sinha S. K., “ Dynamic characteristics of a flexible bladed-rotor with Coulomb damping due to tip-rub”, *Journal of Sound and Vibration*, vol. 273, n° 4-5, p. 875-919, 2004.
- Sundararajan P., Noah S., “ Dynamics of forced nonlinear systems using shooting/arclength continuation method - Application to rotor systems”, *Journal of Vibration and Acoustics*, vol. 119, p. 9-20, 1997.
- Tiwari M., Gupta K., Prakash O., “ Effect of radial internal clearance of a ball bearing on the dynamics of balanced horizontal rotor”, *Journal of Sound and Vibration*, vol. 238, n° 5, p. 723-756, 2000.

